The Energy Flux of Internal Gravity Waves in the Lower Solar Atmosphere

Thomas Straus[1], Bernhard Fleck[2], Stuart M. Jefferies[3], Gianna Cauzzi[4], Scott W. McIntosh[5], Kevin Reardon[4], Giuseppe Severino[1], Matthias Steffen[6]

ABSTRACT

Stably stratified fluids, such as stellar and planetary atmospheres, can support and propagate gravity waves. On Earth these waves, which can transport energy and momentum over large distances and can trigger convection, contribute to the formation of our weather and global climate. Gravity waves also play a pivotal role in planetary sciences (e.g. Young et al. 1997) and modern stellar physics (Charbonnel & Talon 2007). They have also been proposed as an agent for the heating of stellar atmospheres and coronae (Mihalas & Toomre 1981), the exact mechanism behind which is one of the outstanding puzzles in solar

[1]INAF / Osservatorio Astronomico di Capodimonte, Via Moiariello 16, 80131 Napoli, Italy
straus@oacn.inaf.it,severino@oacn.inaf.it

[2]ESA Science Operations Department, c/o NASA Goddard Space Flight Center, Mailcode 671.1, Greenbelt, MD 20771, USA
bfleck@esa.nascom.nasa.gov

[3]Institute for Astronomy, University of Hawaii, 34 Ohia Ku Street, Pukalani, HI 96768, USA
stuartj@ifa.hawaii.edu

[4]INAF / Osservatorio Astrofisico di Arcetri, Largo Enrico Fermi 5, 50125 Firenze, Italy
gcauzzi@arcetri.astro.it,kreardon@arcetri.astro.it

[5]High Altitude Observatory, National Center for Atmospheric Research, P.O. Box 3000, Boulder, CO 80307, USA
mscott@ucar.edu

[6]Astrophysikalisches Institut Potsdam, An der Sternwarte 16, D-14482 Potsdam, Germany
msteffen@aip.de

and stellar physics. Using a combination of high quality observations and 3-D numerical simulations we have the first unambiguous detection of propagating gravity waves in the Sun's (and hence a stellar) atmosphere. Moreover, we are able to determine the height dependence of their energy flux and find that at the base of the Sun's chromosphere it is around 5 kW/m^2. This amount of energy is comparable to the radiative losses of the entire chromosphere and points to internal gravity waves as a key mediator of energy into the solar atmosphere.

Subject headings: hydrodynamics – waves – Sun: atmospheric motions – Sun: chromosphere – Sun: photosphere

1. Introduction

Internal Gravity Waves (IGWs) play an important role in mixing material and transporting energy and momentum in planetary atmospheres, oceans, and the radiative interior of solar-type stars. In the Earth's atmosphere IGWs have been observed and modeled for many years, both in the lower atmosphere (e.g. Eckermann & Preusse 1999; Shindell 2003) as well as at ionospheric heights (e.g. Crowley & Williams 1987). Moreover, IGWs play an important role in the coupling of these two regions. In the oceans IGWs power the overturning meridional circulation that affects pollutant disposal, marine productivity and global climate (e.g. Alford 2003). Elsewhere in the solar system IGWs have been detected on Mars (Seiff & Kirk 1976) and Jupiter (Young et al. 1997; Reuter et al. 2007). In fact, Young et al. (1997) found that the viscous damping of IGWs on Jupiter could explain the enigmatic temperature structure of the planet's thermosphere, solving one of the long-standing problems in planetary physics. In astrophysics, IGWs, stochastically excited by overshooting convection, have been invoked to explain the uniform rotation of the solar core (Gough 1997) and the rotation profile and the surface Lithium abundance of solar-type stars (Charbonnel & Talon 2005). IGWs have also been proposed as an agent for the mechanical heating of stellar atmospheres and coronae more than 25 years ago (Mihalas & Toomre 1981). However the difficulties associated with directly observing them in our closest star, the Sun, have resulted in their neglect in this matter.

The two main theories that have been advanced as viable heating mechanisms of the Sun's chromosphere (and corona) are mechanical heating by upward-propagating waves (Alfvén 1947; Schwarzschild 1948) and Joule heating associated with magnetic field reconnection and the resistive dissipation of electric currents (Parker 1988; Rabin & Moore 1984). Recent results have shown that the Joule heating mechanisms are likely too weak to heat the solar chromosphere (Socas-Navarro 2005), as are high-frequency acoustic waves (Fossum & Carlsson 2005; Carlsson et al. 2007), the main contender for wave heating during the past three decades. If wave heating is the prime candidate, this leaves magnetic waves (e.g. Alfvén) and gravity waves. Interestingly, Alfvén waves have been recently identified in spicules in the upper chromosphere with sufficient energy to accelerate the solar wind and possibly heat the corona (De Pontieu et al. 2007).

Previous efforts in studying the contributions of hydrodynamic waves to the heating of the Sun's outer atmosphere have focused mainly on two areas: the analysis of Doppler shift and intensity time series in the time/frequency domain on the observational side (see e.g. references in Krijger et al. 2001) and — as far as high frequency acoustic waves are concerned — on 1-D numerical simulations (Ulmschneider et al. 2005) on the theoretical side. Recently, three-dimensional, time-dependent radiation hydrodynamics simulations have reached a level of sophistication that allows a direct confrontation of such models with real stellar atmospheres (e.g. Asplund et al. 1997; Stein & Nordlund 1998; Skartlien et al. 2000; Wedemeyer et al. 2004; Vögler et al. 2005). Here, by combining state-of-the-art 3-D simulations of the Sun's atmosphere and similarly advanced high-quality observations, we demonstrate that the influence of gravity waves on the energetics and structure of the outer solar atmosphere must be substantial. (From here on we will use the term atmospheric gravity waves in order to distinguish these internal gravity waves in the solar atmosphere from resonant g modes in the Sun's interior.)

2. Simulations

Three-dimensional, time-dependent, radiation-hydrodynamical simulations of the solar surface convection provide a physical description of the dynamics and energetics of the complex interface between the Sun's convection zone and its overlying radiative atmosphere. Such simulations allow us to study the excitation and propagation of various types of waves by turbulent convective flows. Here we use the simulated wave signatures to make a direct comparison with observations. Moreover, after performing a detailed test between simulated and observed wave spectra, we take advantage of the fact that the simulations provide access to physical parameters not directly accessible through observation.

The 3-D radiation hydrodynamics code used in this work was CO^{5}BOLD (Wedemeyer et al. 2004)[1]. This code solves the coupled non-linear equations of compressible hydrodynamics in an external gravity field together with the non-local radiative energy transport on a fixed 3-D Cartesian grid with 200×200×250 cells that defines the simulated region. The

[1]For a detailed documentation see http://www.astro.uu.se/~bf/co5bold_main.html

physical size of this region is 11.4×11.4 Mm and assumes periodic lateral boundaries. The transmitting upper boundary of the region is located at a height of approximately 900 km above the simulated visible solar surface, while the open lower boundary lies some 4.3 Mm below. A pre-tabulated equation of state accounts for partial ionization and molecule formation and radiative transfer is based on realistic opacities adapted from a recent version of the MARCS stellar atmosphere package (Plez et al. 1992; Asplund et al. 1997; Gustafsson et al. 2003).

We extract the vertical velocity and gas pressure on all of the grid points above the simulated photosphere from 2048 30 seconds time steps of the simulation, corresponding to ∼17 hours of solar time. Choosing two representative heights in the simulation (70 and 250 km; see below), we compute the temporal velocity-velocity (V-V) phase differences between the vertical velocities at two heights to infer the dispersion relation $\mathrm{k_z}(\mathrm{k_h}, \omega)$ of the waves present. We find the waves contained in the simulation to be in excellent agreement with V-V phase relationships determined from observations at approximately the same heights of the solar atmosphere (Fig. 1). We use this agreement to demonstrate that our simulation captures the basic properties of the dynamics of the Sun's atmosphere and can therefore be used for the subsequent investigation with a high degree of reliability.

Applying a 3-D Fourier transform (in x, y, and t) to each layer of the simulation we can separate the different wave phenomena in the k-ω diagram. We then estimate the mechanical energy flux at every point $(\mathrm{k_h}, \omega)$ given by the temporal average of the product of the corresponding pressure fluctuation and vertical velocity $\langle \mathrm{p_1}(\mathrm{k_h}, \omega)\, \mathrm{v_z}(\mathrm{k_h}, \omega)\rangle$. A map of the energy flux at 600 km above the photosphere near the base of the chromosphere shows the largest upward directed energy flux in the region of progressive atmospheric gravity waves, where we also observe downward directed phase propagation (Fig. 2). The opposite directions of energy flux and phase propagation is the classical signature of propagating internal gravity waves (Lighthill 1978). We also note that Fig. 2 shows a strong contribution to the vertical energy flux from the "fundamental mode" (a resonant surface gravity mode) traced out by the parabolic path $\omega = \sqrt{g\mathrm{k_h}}$ (Fig. 1). While energetically about an order of magnitude less important than the gravity waves, this is a remarkable finding, as the f-mode is not expected to transport energy in the vertical direction. This is not the only surprising property of the f-mode. Being an incompressible surface mode, it should not appear in intensity oscillations, in contradiction to observations, where it appears as a prominent feature in $k - \omega$ power spectra (e.g. as beautifully demonstrated in Mitra-Kraev et al. 2008). The f-mode obviously merits further investigation.

We determine the total energy flux of atmospheric gravity waves in the simulation by integrating $\langle \mathrm{p_1}\, \mathrm{v_z}\rangle$ at each height over all points with downward phase propagation. These values, along with those for the simulated acoustic flux, are summarized in Fig. 3. The height dependence of the gravity wave energy flux agrees with an earlier prediction (Mihalas & Toomre 1982) and, at the base of the chromosphere, the flux is comparable to the net radiative losses of the quiet chromosphere ($\sim$4.3 $\mathrm{kWm^{-2}}$; see Vernazza et al. 1976). The simulated acoustic flux, on the other hand, is about a factor of ten smaller, consistent with recent reports (Fossum & Carlsson 2005; Carlsson et al. 2007).

3. Observations

We now turn our attention from simulations to wave properties observed in quiet sun regions (at solar disk center) with three different high-resolution instruments: Interferometric BIdimensional Spectrometer (IBIS, Cavallini 2006) and the Echelle Spectrograph, which both operate at the Dunn Solar Telescope (DST) of the Sacramento Peak National Solar Observatory, and the Michelson Doppler Imager (MDI, Scherrer et al. 1995) on SOHO.

The IBIS data set consists of a high resolution time series of spectral scans of the mid-photospheric Fe *I* 7090Å line, taken under good seeing conditions in a quiet region at Sun centre on May 31, 2004 (Janssen & Cauzzi 2006). The spatial resolution is 120 km/pixel, time cadence 19 seconds, and the duration of the series 55 minutes. At each spatial position in the 55 Mm diameter field-of-view, line-of-sight velocities were calculated for two heights in the 7090 line from the Dopplershift of the line core (formed at approximately 250 km), and from the center-of-gravity of line wings in the range 8-16 pm from the line core. The Echelle spectrograph data are approximately 4-hour long time series of Na *I* $\mathrm{D_1}$ and Mg *I* $\mathrm{b_2}$ in combination with photospheric Fe *I* lines (Deubner & Fleck 1989). These spectral lines are formed at heights between 150 km and 750 km (see Table 1). The MDI data set is an 15-hour time series (Straus et al. 1999) of high-resolution Doppler velocity measurements in the Ni *I* 6768Å absorption line, which forms at about 100 km height. The analysis has been limited to the first 8.5 hours of the time series which covers a field-of-view of 300 Mm$\times$300 Mm at a resolution of 725 km/pixel. The time cadence is 60 seconds.

Since pressure fluctuations are not directly observable we determine the observational energy flux from the product of the plasma density (ρ_0, given by VAL model C, Vernazza et al. 1976), the mean squared velocity amplitude ($\langle \mathrm{v}^2 \rangle$) and the vertical component of the group velocity ($\mathrm{v_{g,z}(k_h,\omega)}$). As our observations are taken at disk centre, we measure only the vertical component $\mathrm{v_z = v}\cos(\theta)$ of the velocity fluctuations; $\langle \mathrm{v}^2 \rangle$ then results from $\langle \tilde{\mathrm{V}}_\mathrm{z}(\mathrm{k_h},\omega) \cdot \tilde{\mathrm{V}}^*_\mathrm{z}(\mathrm{k_h},\omega) \rangle / \cos^2(\theta)$, where θ is the angle between the horizontal and the wave vector $\mathbf{k}$ and is given by $\cos(\theta) = \omega/\omega_\mathrm{BV}$, $\tilde{\mathrm{V}}_\mathrm{z}(\mathrm{k_h},\omega)$ is the Fourier transform of the velocity perturbations, * denotes the complex conjugate, and ω_BV is the Bruunt-Väisälä frequency.

Using 7.5 km/s for the speed of sound, obtained from a fit of the high frequency part of the V-V phase spectrum $\Phi(\mathrm{k_h}, \omega)$ between the two heights in the IBIS data set to a theoretical spectrum following the theory of linear waves (Souffrin 1966), and $\gamma = 5/3$ we obtain $\omega_{\mathrm{BV}}/2\pi$=4.75 mHz. We then fitted a surface to the gravity wave regime of the V-V phase spectrum, again following the theory of linear waves. As the lowest frequencies (below 0.7 mHz) show the signature of convective motions, we excluded these for our estimate, as we did with waves above the Lamb line $\omega = \mathrm{c\,k_h}$. Using the relations for the phase travel time $TT_{\mathrm{ph}} = \frac{\Phi(\mathrm{k_h},\omega)}{360^\circ} \cdot \frac{2\pi}{\omega}$ and the phase velocity $\mathrm{v_{Ph,z}} = \Delta z/TT_{\mathrm{ph}}$, with Δz=180 km between the core and wing of the iron line estimated from the slope of the linear phase delay in the high frequency part of the phase spectrum, we can determine the vertical group velocity $\mathrm{v_{g,z}}$=-$\mathrm{v_{Ph,z}}\ \sin^2(\theta)$ and thus measure all factors $\rho_0\ \langle \mathrm{v}^2 \rangle\ \mathrm{v_{g,z}}(\mathrm{k_h}, \omega)$ that determine the vertical energy flux of gravity waves. The results are given in Fig. 3 and Table 1.

As the Ni line of the MDI data set is formed in the lower photosphere close to the Fe line of the IBIS data set, we adopt the above value for $\mathrm{v_{g,z}}(\mathrm{k_h}, \omega)$ to determine the energy flux at the level of the Ni line. We note that this value agrees remarkably well with that derived using a completely independent method: The large field-of-view of the MDI data permits to estimate both the vertical and horizontal components of $\langle \mathrm{v}^2 \rangle$, and therefore the geometry of the oscillations. The horizontal phase speed can be measured directly in filtered x-t space-time slices, which in turn yields the vertical group velocity $\mathrm{v_{g,z}}$.

We also estimate the energy flux due to atmospheric gravity waves and acoustic waves at various heights from the 1-D spectrograph data. Again, like in the case of the 2-D observations, frequencies below 0.7 mHz have been excluded from our estimate, as the velocity signal shows contamination by convection. Furthermore, 1-D observations do not allow a clean decomposition of horizontal wavelengths, as the angle of wave propagation with respect to the slit is unknown. Therefore, to avoid contamination by p-modes, the 1-D observations have been integrated only between 0.7 and 2.1 mHz and then corrected to the entire range of 0.7 - 5 mHz, based on the flux ratio between both frequency ranges we find in the simulations. We consider the results from the 1-D data only a lower limit. We emphasize that the 2-D observations do not suffer such limitations and that the flux estimates based on the 2-D observations are completely independent from the flux estimates obtained from the simulation.

4. Conclusions

The observational results shown in Fig. 3 are in good agreement with those determined independently from our simulation and confirm that low-frequency atmospheric gravity waves are energetically more important for the lower solar atmosphere than high-frequency acoustic waves. Lastly, from the MDI data we find that the dominant component of the gravity wave spectrum is inclined by about 70° with respect to the vertical. Thus, the values in Figure 3 represent only 30% of the total energy flux due to atmospheric gravity waves. The remaining 70% is transported horizontally and might become important in mode conversion of these waves to Alfvén waves when they encounter magnetic structures. The conversion of gravity waves into Alfvén waves is an efficient process (Lighthill 1967). This, together with the fact that the IBIS and MDI data show significantly suppressed atmospheric gravity waves at locations of magnetic flux (Fig. 4), and the recent discovery of ubiquitous Alfvén waves in the Sun's outer atmosphere (Tomczyk et al. 2007; De Pontieu et al. 2007) lead us to speculate that the mode conversion scenario may be in play. We conclude that atmospheric gravity waves represent a crucially important energy mediator in the quiet, lower atmosphere of the Sun.

The simulations were carried out at CINECA (Bologna/Italy) with CPU time assigned under INAF/CINECA agreement 2006/2007. Th.S. acknowledges financial support by E-SA and ASI. S.M.J. was supported by NSF award 0632399. IBIS has been built by IN-AF/Osservatorio Astrofisico di Arcetri with contributions from the Università di Firenze and the Università di Roma "Tor Vergata". IBIS construction and operation has been supported by the Italian Ministero dell'Università e della Ricerca (MUR) as well as the Italian Ministry of Foreign Affairs (MAE). NSO is operated by the Association of Universities for Research in Astronomy, Inc. (AURA), under cooperative agreement with the National Science Foundation. SOHO is a project of international cooperation between ESA and NASA.

Facilities: Dunn () SOHO ()

REFERENCES

Alford, M. H. 2003, Nature, 423, 159

Alfvén, H. 1947, MNRAS, 107, 211

Asplund, M., Gustafsson, B., Kiselman, D., & Eriksson, K. 1997, A&A, 318, 521

Carlsson, M., Hansteen, V. H., de Pontieu, B., McIntosh, S., Tarbell, T. D., Shine, D., Tsuneta, S., Katsukawa, Y., Ichimoto, K., Suematsu, Y., Shimizu, T., & Nagata, S. 2007, Publ. Astron. Soc. Japan, 59, 663

Cavallini, F. 2006, Sol. Phys., 236, 415

Charbonnel, C. & Talon, S. 2005, Science, 309, 2189

—. 2007, Science, 318, 922

Crowley, G. & Williams, P. J. S. 1987, Nature, 328, 231

De Pontieu, B., McIntosh, S. W., Carlsson, M., Hansteen, V. H., Tarbell, T. D., Schrijver, C. J., Title, A. M., Shine, R. A., Tsuneta, S., Katsukawa, Y., Ichimoto, K., Suematsu, Y., Shimizu, T., & Nagata, S. 2007, Science, 318, 1574

Deubner, F.-L. & Fleck, B. 1989, A&A, 213, 423

Eckermann, S. D. & Preusse, P. 1999, Science, 286, 1534

Fossum, A. & Carlsson, M. 2005, Nature, 435, 919

Gough, D. 1997, Nature, 388, 324

Gustafsson, B., Edvardsson, B., Eriksson, K., Mizuno-Wiedner, M., Jørgensen, U. G., & Plez, B. 2003, in Astronomical Society of the Pacific Conference Series, Vol. 288, Stellar Atmosphere Modeling, ed. I. Hubeny, D. Mihalas, & K. Werner, 331

Janssen, K. & Cauzzi, G. 2006, A&A, 450, 365

Krijger, J. M., Rutten, R. J., Lites, B. W., Straus, T., Shine, R. A., & Tarbell, T. D. 2001, A&A, 379, 1052

Lighthill, M. F. 1967, in Aerodynamic Phenomena in Stellar Atmospheres, IAUS 28, 429

Lighthill, J. 1978, Waves in Fluids (Cambridge Univ. Press)

Mihalas, B. W. & Toomre, J. 1981, ApJ, 249, 349

—. 1982, ApJ, 263, 386

Mitra-Kraev, U., Kosovichev, A. G., & Sekii, T. 2008, A&A, 481, L1

Parker, E. N. 1988, ApJ, 330, 474

Plez, B., Brett, J. M., & Nordlund, A. 1992, A&A, 256, 551

Rabin, D. & Moore, R. 1984, ApJ, 285, 359

Reuter, D. C., Simon-Miller, A. A., Lunsford, A., Baines, K. H., Cheng, A. F., Jennings, D. E., Olkin, C. B., Spencer, J. R., Stern, S. A., Weaver, H. A., & Young, L. A. 2007, Science, 318, 223

Scherrer, P. H., Bogart, R. S., Bush, R. I., Hoeksema, J. T., Kosovichev, A. G., Schou, J., Rosenberg, W., Springer, L., Tarbell, T. D., Title, A., Wolfson, C. J., Zayer, I., & MDI Engineering Team. 1995, Sol. Phys., 162, 129

Schwarzschild, M. 1948, ApJ, 107, 1

Seiff, A. & Kirk, D. B. 1976, Science, 194, 1300

Shindell, D. 2003, Science, 299, 215

Skartlien, R., Stein, R. F., & Nordlund, Å. 2000, ApJ, 541, 468

Socas-Navarro, H. 2005, ApJ, 633, L57

Souffrin, P. 1966, Annales d'Astrophysique, 29, 55

Stein, R. F., & Nordlund, A. 1998, ApJ, 499, 914

Straus, T., Severino, G., Deubner, F.-L., Fleck, B., Jefferies, S. M., & Tarbell, T. 1999, ApJ, 516, 939

Tomczyk, S., McIntosh, S. W., Keil, S. L., Judge, P. G., Schad, T., Seeley, D. H., & Edmondson, J. 2007, Science, 317, 1192

Ulmschneider, P., Rammacher, W., Musielak, Z. E., & Kalkofen, W. 2005, ApJ, 631, L155

Vernazza, J. E., Avrett, E. H., & Loeser, R. 1976, ApJs, 30, 1

Vögler, A., Shelyag, S., Schüssler, M., Cattaneo, F., Emonet, T., & Linde, T. 2005, A&A, 429, 335

Wedemeyer, S., Freytag, B., Steffen, M., Ludwig, H.-G., & Holweger, H. 2004, A&A, 414, 1121

Young, L. A., Yelle, R. V., Young, R., Seiff, A., & Kirk, D. B. 1997, Science, 276, 108

This preprint was prepared with the AAS LaTeX macros v5.2.

Table 1. Energy flux estimates from observations.

	2-D data			1-D data					
	Ni 6768	Fe 7090 (wing)	Fe 7090 (core)	Fe 5929	Fe 8947	Fe 5930	Fe 6302	Mg b2	Na D1
height	100	70	250	150	200	330	350	690	750
acoustic waves	2.5	11.9	1.4	7.8	5.0	1.4	0.9	0.4	0.3
atmospheric gravity waves	28.6	126	20.8	124	71.7	26.4	18.6	0.5	0.3
correction factor				1.07	1.35	1.86	1.87	2.11	2.10

Note. — Height is given in km above the base of the photosphere; flux values are in kW/m^2. The 1-D data has been integrated from 0.7 to 2.1 mHz and then multiplied by the given correction factor determined from the simulation to consider the full AGW frequency range from 0.7 to 5 mHz.

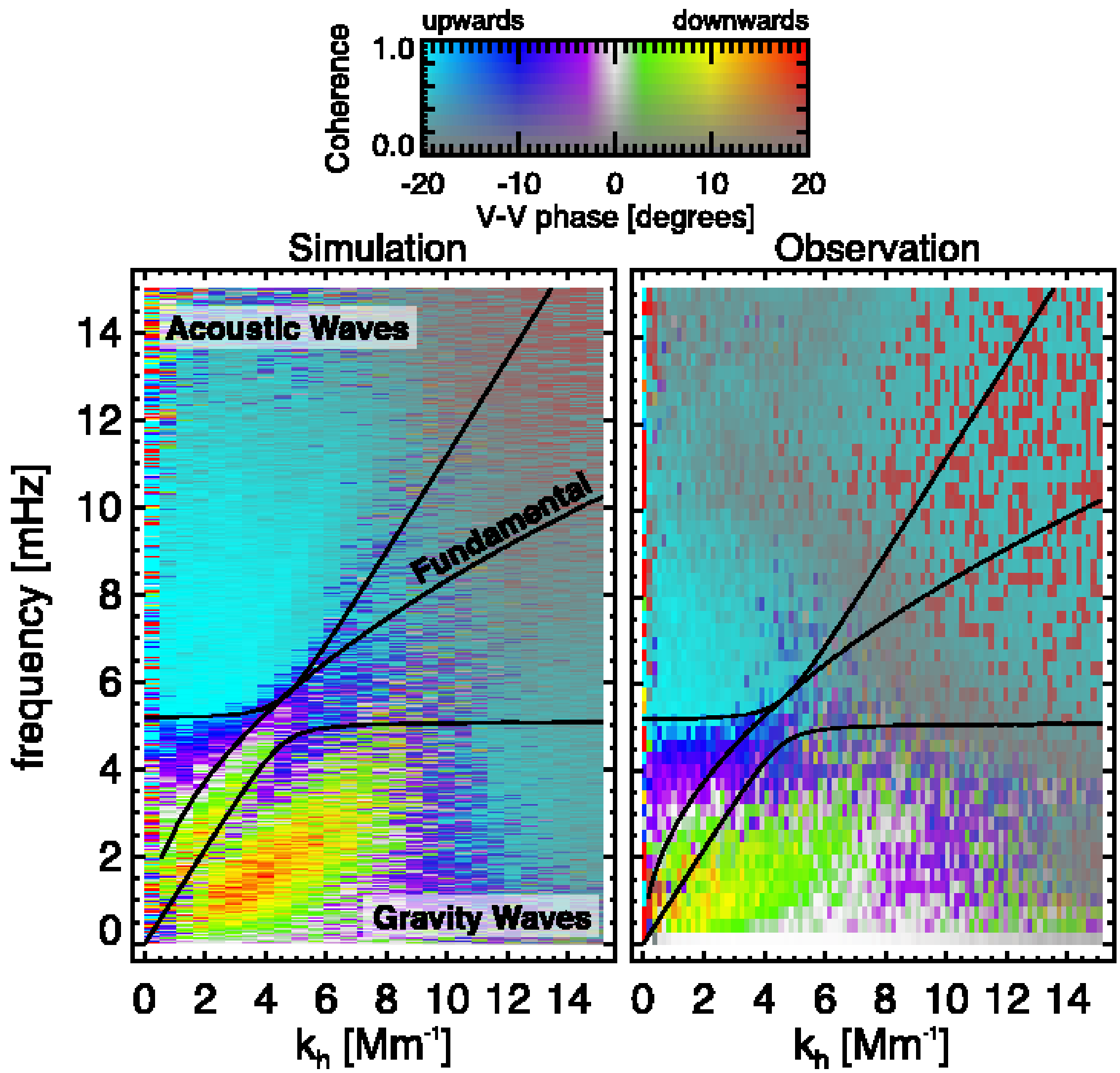

Fig. 1.— Simulated (left) and observed (right) 2-D V-V phase difference: A 3D Fast Fourier Transform (FFT) has been applied to both the simulated and observed vertical velocity v_z(x,y,t) at the heights of 250 km and 70 km. Assuming spatial isotropy in (k_x,k_y), the complex cross power is integrated over $k_h^2 = k_x^2 + k_y^2$, and the phase $\Phi(k_h, \omega)$ determined, where $\omega = 2\pi\nu$. The results of the simulations (left) are in remarkable agreement with the high-resolution IBIS observations (right). Both observations and simulations clearly identify the region of downward phase propagation at low frequencies, known from 1-D observations (Deubner & Fleck 1989), with the region of propagating atmospheric gravity waves in the k-ω spectrum. The black lines indicate the fundamental mode and the diagnostic diagram, which separates the various wave regimes.

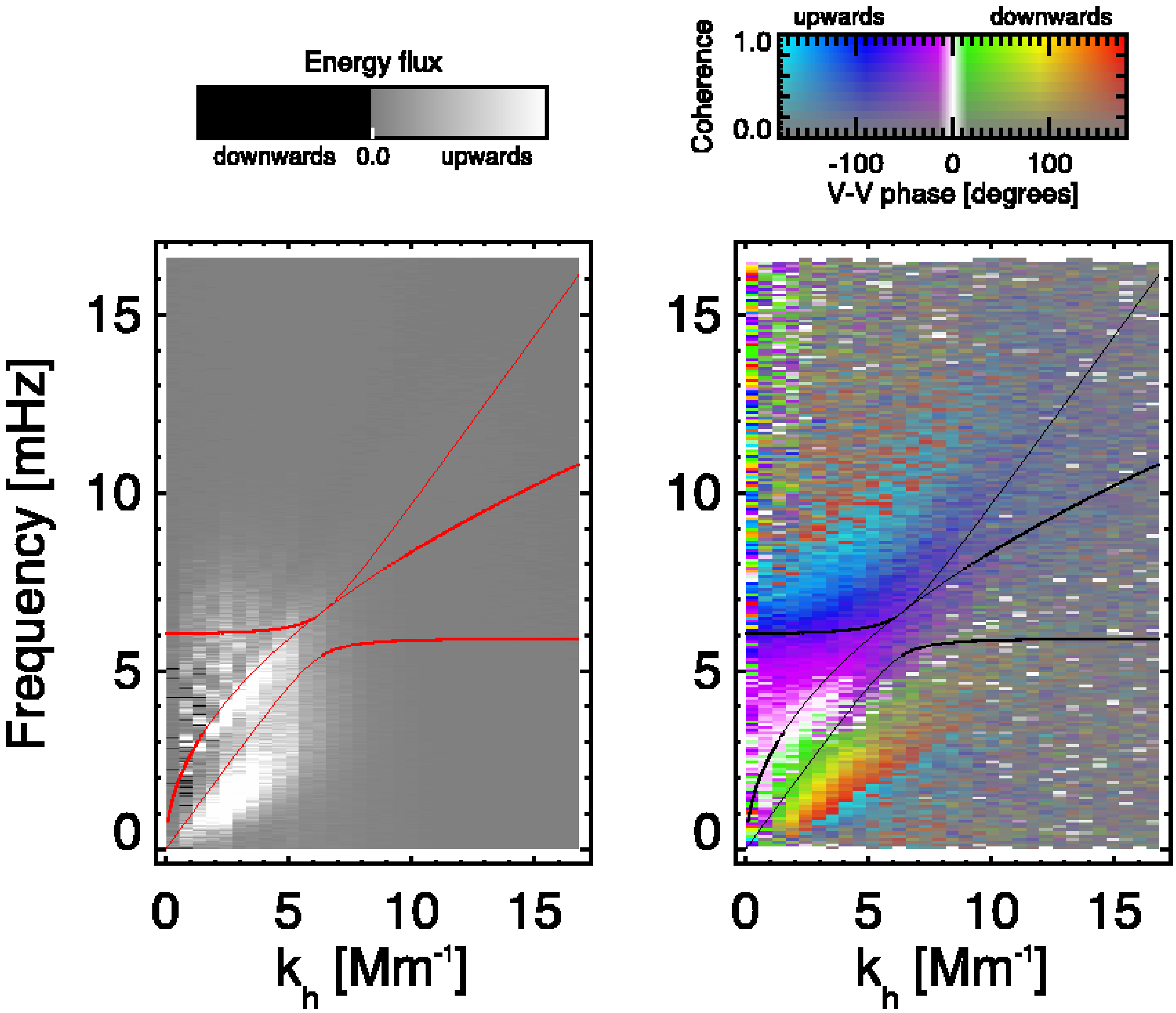

Fig. 2.— Energy flux (left) and V-V phase difference (right) in the k-ω diagram in the simulation: A 3-D Fast Fourier Transform (FFT) has been applied to the simulated vertical velocity v_z(x,y,t) and gas pressure p_1(x,y,t) at two heights: 150 km and 600 km. Assuming spatial isotropy in (k_x,k_y), the mechanical energy flux at 600 km is integrated over $k_h^2 = k_x^2 + k_y^2$ (left panel), and the V-V phase difference is determined between the two levels (right panel).

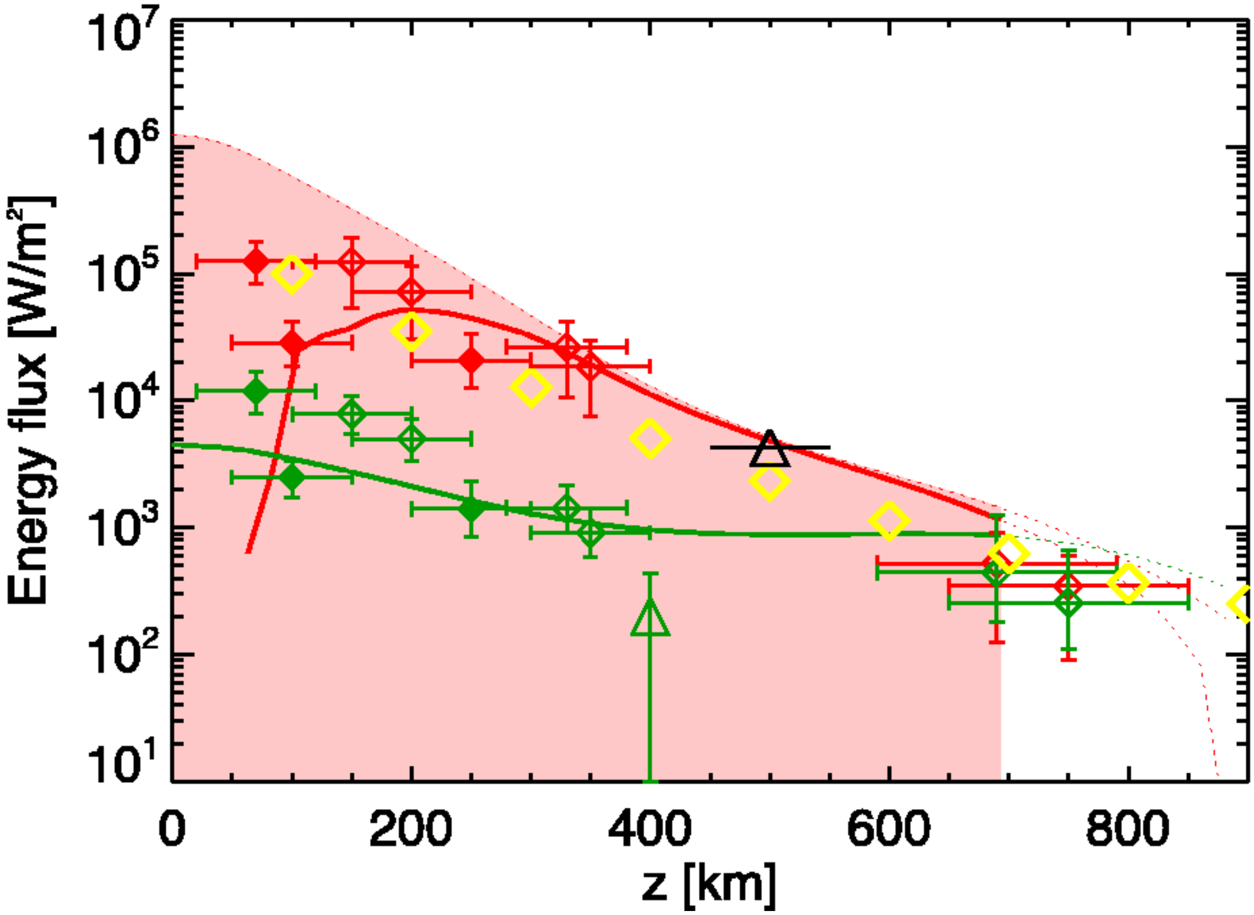

Fig. 3.— Simulated and observed energy flux as a function of height, compared to total radiative losses of the chromosphere: The flux of atmospheric gravity waves and acoustic waves are displayed in red and green, respectively. The black triangle represents the total radiative losses of the chromosphere (Vernazza et al. 1976), marked at the base of the chromosphere. The lines represent results from our simulation, the diamond symbols the observations as given in Table 1. Filled and open symbols are from 2-D and 1-D observations, respectively. The green triangle gives a recent upper limit estimate for the acoustic flux (Fossum & Carlsson 2005). The red shaded area gives the total flux of the region of propagating atmospheric gravity waves without constraint on phase difference. The yellow diamonds represent an earlier prediction of the height dependence of the energy flux of atmospheric gravity waves (Mihalas & Toomre 1982).

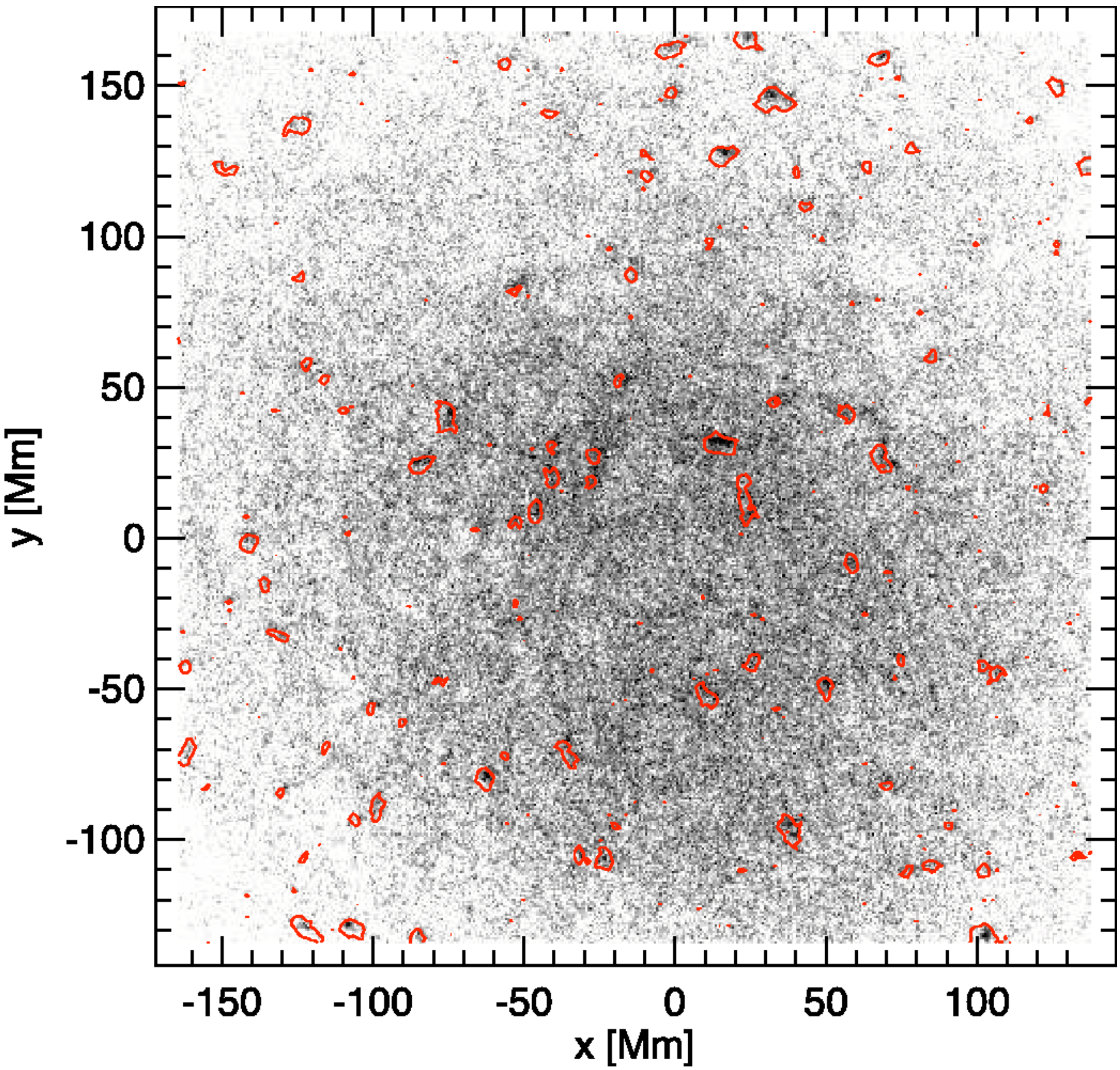

Fig. 4.— Spatial variations of the RMS velocity of atmospheric gravity waves obtained from the MDI data (grayscale), overlayed by the 35 G contour lines from a co-temporal MDI magnetogram (red contours). Processed IBIS and MDI time lapse movies showing internal gravity waves are available at http://www.oacn.inaf.it/∼straus/04_science/ApJL2008/ and http://zeus.nascom.nasa.gov/∼bfleck/Publications/Movies/GravityWaves/